The Astrophysical Journal, 908:181 (11pp), 2021 February 20 https://doi.org/10.3847/1538-4357/abd254

Tracing Dark Energy History with Gamma-Ray Bursts

M. Muccino[1,2], L. Izzo[3], O. Luongo[2,4,5], K. Boshkayev[2,6,7], L. Amati[8], M. Della Valle[9], G. B. Pisani, and E. Zaninoni

[1] INFN, Laboratori Nazionali di Frascati, Via Enrico Fermi, 54, I-00044, Frascati (RM), Italy; marco.muccino@lnf.infn.it
[2] NNLOT, Al-Farabi Kazakh National University, Al-Farabi ave. 71, 050040 Almaty, Kazakhstan; orlando.luongo@unicam.it, kuantay@mail.ru
[3] DARK, Niels Bohr Institute, University of Copenhagen, Lyngbyvej 2, DK-2100 Copenhagen, Denmark; luca.izzo@nbi.ku.dk
[4] Dipartimento di Matematica, Università di Pisa, Largo B. Pontecorvo 5, Pisa, I-56127, Italy
[5] Divisione di Fisica, Università di Camerino, Via Madonna delle Carceri, 9, I-62032, Italy
[6] Department of Physics, Nazarbayev University, 53 Kabanbay Batyr ave., 010000 Nur-Sultan, Kazakhstan
[7] Department of Engineering Physics, Satbayev University, 22 Satbayev str., 050013 Almaty, Kazakhstan
[8] INAF, Istituto di Astrofisica Spaziale e Fisica Cosmica, Bologna, Via Gobetti 101, Bologna, I-40129, Italy
[9] INAF, Osservatorio Astronomico di Capodimonte, Salita Moiariello 16, Napoli, I-80131, Italy
Received 2020 November 5; revised 2020 December 4; accepted 2020 December 8; published 2021 February 23

Abstract

Observations of gamma-ray bursts up to $z \sim 9$ are best suited to study the possible evolution of the universe equation of state at intermediate redshifts. We apply the Combo relation to a sample of 174 gamma-ray bursts to investigate possible evidence of evolving dark energy parameter $w(z)$. We first build a gamma-ray burst Hubble's diagram and then we estimate the set $(\Omega_m, \Omega_\Lambda)$ in the framework of flat and non-flat ΛCDM paradigm. We then get bounds over the wCDM model, where w is thought to evolve with redshift, adopting two priors over the Hubble constant in tension at 4.4σ, i.e., $H_0 = (67.4 \pm 0.5)$ km s^{-1} Mpc^{-1} and $H_0 = (74.03 \pm 1.42)$ km s^{-1} Mpc^{-1}. We show our new sample provides tighter constraints on Ω_m since at $z \leqslant 1.2$ we see that $w(z)$ agrees within 1σ with the standard value $w = -1$. The situation is the opposite at larger z, where gamma-ray bursts better fix $w(z)$ that seems to deviate from $w = -1$ at 2σ and 4σ level, depending on the redshift bins. In particular, we investigate the $w(z)$ evolution through a piecewise formulation over seven redshift intervals. From our fitting procedure we show that at $z \geqslant 1.2$ the case $w < -1$ cannot be fully excluded, indicating that dark energy's influence is not negligible at larger z. We confirm the Combo relation as a powerful tool to investigate cosmological evolution of dark energy. Future space missions will significantly enrich the gamma-ray burst database even at smaller redshifts, improving *de facto* the results discussed in this paper.

Unified Astronomy Thesaurus concepts: Standard candles (1563); Dark energy (351); Gamma-ray bursts (629)

Supporting material: machine-readable table

1. Introduction

In the cosmological concordance model, the universe is approximated by ∼30% of baryonic and cold dark matter and by ∼70% of an exotic form of constant *dark energy* (DE, see e.g., Planck Collaboration et al. 2020, hereafter P20). In particular, to speed up the universe today, DE counterbalances the action of gravity through a negative pressure. Recent observations at small redshifts favor a cosmological constant contribution, Λ, to evolving DE, albeit recent observations provided by Planck Collaboration et al. (2020) seem to show unexpected tensions among observables, not yet understood within the concordance paradigm, dubbed the ΛCDM model. In the latter, the corresponding equation of state (EoS) turns out to be *exactly* $w \simeq -1$ (P20; Riess et al. 2007). Any deviations from $w = -1$ would lead to more complicated versions of DE fluids or to extended and/or modified theories of gravity still objects of debate (Bronstein 1933; Tsujikawa 2013; Sahni et al. 2014; Ding et al. 2015; Capozziello et al. 2019).

Several methods have been proposed to investigate a possible evolution of $w(z)$ with the redshift, mainly involving supernovae (SNe) Ia (Phillips 1993; Perlmutter et al. 1998, 1999; Riess et al. 1998; Schmidt et al. 1998) and/or standard candles and rulers. However, the shortage of data at high redshifts ($z \geqslant 1$) inevitably brings large uncertainties over w measurements (Suzuki et al. 2012), providing an unvoidable degeneracy problem among cosmological models. For example, the simplest ΛCDM generalization is based on a first-order approximation, $w(z) = w_0 + w_a z/(1+z)$ (Chevallier & Polarski 2001; Linder 2003) fully degenerating with several other redshift-binned parameterizations within the sphere $z < 1$ (see, e.g., King et al. 2014).

Gamma-ray bursts (GRBs) have the advantage over other cosmological probes and rulers to homogeneously cover a large interval of redshift up to $z \approx 9$ (Cucchiara et al. 2011; Salvaterra et al. 2012) and their redshift distribution peaks at $z \sim 2$–2.5 (Coward et al. 2013), where the farthest SN Ia has been detected (Rodney et al. 2015). In the last decades, the analysis of larger samples has led to various phenomenological correlations between GRB photometric and spectroscopic properties, suggesting possible cosmological applications (see e.g., Schaefer 2007; Amati et al. 2008; Capozziello & Izzo 2008; Dainotti et al. 2008; Izzo et al. 2009; Amati & Della Valle 2013; Wei et al. 2014, and references therein). Recently Izzo et al. (2015) (hereafter I15) developed a method for measuring the cosmological parameters from a sample of 60 GRBs, which minimizes the cosmological "circularity" problem affecting the computation of the luminosity distances in all GRB correlations.[10] This technique is based on the so-called *Combo relation*,[11] which is characterized by a small data scatter and involves prompt and afterglow GRB parameters (Bernardini et al. 2012; Margutti et al. 2013). The "candle" is provided by the plateau X-ray afterglow luminosity L_0, which

[10] For alternative techniques see e.g., (Amati et al. 2019; Capozziello et al. 2020; Luongo & Muccino 2020a).
[11] The name *Combo* states for *combination* since it combines $E_{p,i}$–$E_{\gamma,iso}$ (Amati et al. 2008) and $E_{\gamma,iso}$–$E_{X,iso}$–$E_{p,i}$ relations (Bernardini et al. 2012).

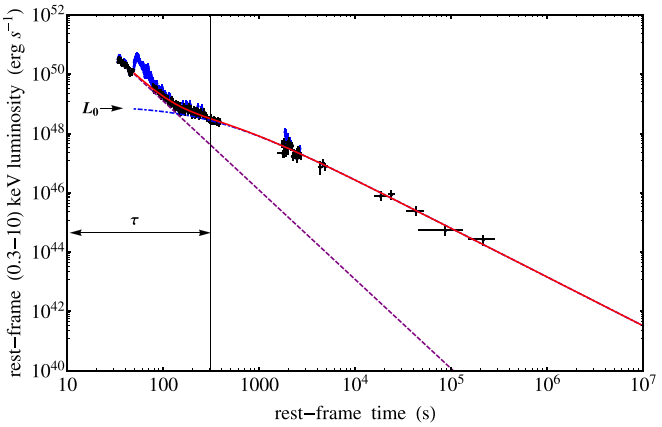

Figure 1. The rest-frame 0.3–10 keV light curve of GRB 060418A. The total fit (red curve) is composed of a steep decay (dashed purple power-law) and a plateau + late power-law decay (dotted–dashed blue curve). The black dots are the data filtered by the flares (blue dots). The vertical black line indicates τ; an arrow marks the luminosity L_0.

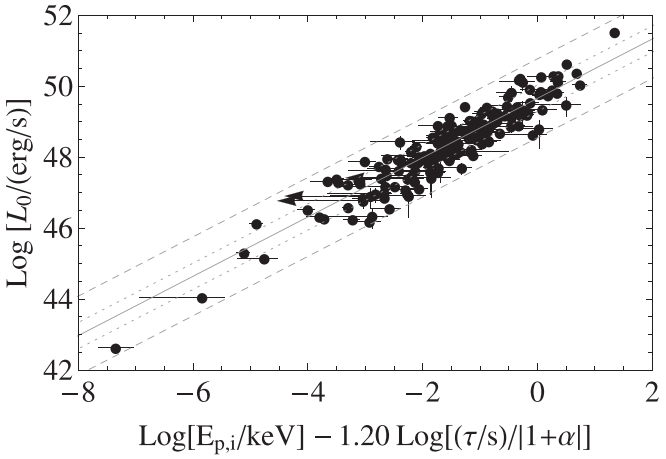

Figure 2. The Combo relation from the sample of 174 GRBs (black circles) in the flat ΛCDM model with indicative values $H_0 = 71$ km s^{-1} Mpc^{-1}, $\Omega_m = 0.27$, and $\Omega_\Lambda = 0.73$. The best-fit (solid gray line) and the 1 and 3σ of extra-scatter (dotted and dashed gray lines) are also displayed.

is related to its rest-frame duration τ, to the late power-law decay index α of the X-ray afterglow luminosity, and to the rest-frame peak energy of the GRB prompt emission $E_{\mathrm{p,i}}$ (see Figure 1). The existence of this relation was later confirmed by Dainotti et al. (2016) where a similar relation based on the use of the peak luminosity has been derived and strongly supported by the existence of the *L–T–E* correlation, recently proposed by Tang et al. (2019) and Xu et al. (2020).

In this work, adopting an extended GRB sample, characterized by a complete data set in gamma- and X-rays, we fix limits over DE's evolution. Our general strategy remarks the same of I15 and aims at getting novel bounds over the whole matter content, i.e., Ω_m. Afterwards, we fix the cosmological constant density, Ω_Λ, testing the validity of the ΛCDM model. Our findings adopt the estimated values of L_0 as distance indicator and can be generalized to any DE scenarios. To this end, we constrain the evolution of $w(z)$ through a piecewise formulation over the GRB redshift intervals. Theoretical discussions of our results are prompted, leading to an overall agreement with the ΛCDM model at small and intermediate redshifts. Outside our time, slight deviations from $w = -1$ are not excluded a priori. Precisely, from our new GRB sample we get tighter constraints on DE's evolution, showing that at $z \leqslant 1.2$ DE turns out to be compatible with a cosmological constant, but beyond $z \simeq 1.2$ it does not since the case $w < -1$ cannot be fully excluded. These deviations are however severely affected by uncertainties and so further space missions, e.g., Space Variable Objects Monitor (SVOM, Cordier et al. 2018), enhanced X-ray Timing and Polarimetry (eXTP, Zhang et al. 2016), and Transient High-Energy Sky and Early Universe Surveyor (THESEUS, Amati et al. 2018), will significantly enrich the GRBs database to remove the ambiguity over the form of $w(z)$ as we discuss later in the manuscript.

The paper is structured as follows. In Section 2, we extend the sample of 60 GRBs in I15 with 114 additional GRBs characterized by a complete data set in gamma- and X-rays up to 2018 December. In Section 3, we provide new constraints on the cosmological parameters Ω_m and Ω_Λ using the estimated values of L_0 as distance indicator. In particular, in Section 4, we constrain the evolution of $w(z)$ by considering a piecewise formulation over the GRB redshift interval. The results of our analysis are then discussed in Section 5, In Section 6 we draw our conclusions.

2. The Updated GRB Sample

2.1. Brief Summary on the Relation and the Updated Sample

The Combo relation writes as (see I15, for details)

$$\log\left(\frac{L_0}{\mathrm{erg\ s^{-1}}}\right) = \log\left(\frac{A}{\mathrm{erg\ s^{-1}}}\right) + \gamma \log\left(\frac{E_{\mathrm{p,i}}}{\mathrm{keV}}\right) - \log\left(\frac{\tau/\mathrm{s}}{|1+\alpha|}\right), \quad (1)$$

where γ is the slope and A the normalization. For each GRB, the rest-frame peak energy $E_{\mathrm{p,i}}$ is inferred from the $\nu F(\nu)$ GRB spectrum, while L_0, τ, and α are inferred by fitting the rest-frame 0.3–10 keV flare-filtered afterglow luminosity light curves with the function $L(t) = (1 + t/\tau)^\alpha$ introduced in Ruffini et al. (2014) (hereafter R14, see, e.g., Figure 1).[12]

From our sample we exclude light curves with $\alpha > -1$, which may have a change in slope beyond the XRT time coverage and/or be polluted by a late flaring activity. We obtain a sample of 174 GRBs, of which 60 are from I15 and 114 are introduced in this work (see Table 4). The Combo relation within the flat ΛCDM model is displayed in Figure 2. Following D'Agostini (2005), we obtain the best-fit parameters: $\log[A/(\mathrm{erg\ s^{-1}})] = 49.66 \pm 0.20$, $\gamma = 0.84 \pm 0.08$, and an extra-scatter $\sigma_{\mathrm{ex}} = 0.37 \pm 0.02$. The corresponding Spearman's coefficient is $\rho_s = 0.92$ and the p-value from the two-sided Student's t-distribution is $p = 1.17 \times 10^{-48}$.

2.2. The Calibration

The Combo relation is calibrated through a two-steps method minimizing the use of SNe Ia (I15). This method is based on:

(1) the determination of γ and σ_{ex} from various, small subsamples of GRBs lying almost at the same redshift;

[12] The flare-filtered luminosity light curves are iteratively fitted with the function in R14: at every iteration, data points with the largest positive residual are discarded, until a final fit with a p-value > 0.3 is obtained.

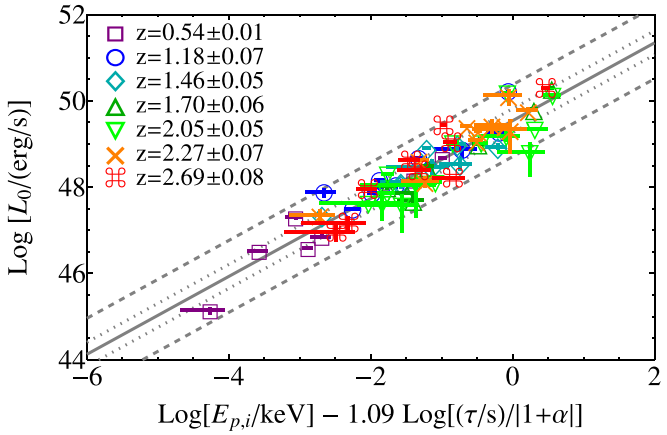

Figure 3. The Combo sub-samples (see legend). The solid gray best-fit line and the dotted (dashed) gray lines at 1σ (3σ) are obtained from the calibrated values of γ and $\sigma_{\rm ex}$ as inferred in Section 2.2.1. The normalization A is constrained to the value determined in Section 2.2.2.

(2) the determination of A from SNe Ia located at the same redshift of the nearest GRBs of the sample.

The use of SNe Ia in the step (2) is limited to the lowest redshift where the effect of the cosmology on the distance modulus of the calibrating SNe Ia is negligible (see Figure 3 in I15).

2.2.1. The Determination of γ and σ_{ex}

To select the GRB sub-samples at the same z with well constrained best-fit parameters, we impose that the corresponding relations must span at least 2 orders of magnitude in the Combo plane. Since in each sub-sample the GRB luminosity distances d_l are approximately the same, instead of using $L_0 = 4\pi d_l^2 F_0$, we employ the rest-frame 0.3–10 keV energy flux F_0, rendering this procedure cosmology-independent. We found seven sub-samples, shown in Figure 3. Their best-fit slope parameters γ_z (see Table 1) exhibit no evident trend with z within the errors, implying that the Combo relation does not result from an evolution effect. This feature allows us to assume that the above seven sub-samples do follow the same correlation with the same γ and $\sigma_{\rm ex}$ but different normalizations. Therefore, we perform a simultaneous fit of the above sub-samples requiring γ and $\sigma_{\rm ex}$ to be the same for all of them. The best-fit values, which minimize the sum of the seven log-likelihood functions, are $\gamma = 0.90 \pm 0.13$ and $\sigma_{\rm ex} = 0.28 \pm 0.03$ (see Figure 3).

2.2.2. The Calibration of A

The Combo relation distance modulus is (see, e.g., I15),

$$\mu_{\rm GRB} = -97.45 + \frac{5}{2}\left[\log\left(\frac{A}{\rm erg\ s^{-1}}\right) + \gamma \log\left(\frac{E_{\rm p,i}}{\rm keV}\right) - \log\left(\frac{\tau/{\rm s}}{|1+\alpha|}\right) - \log\left(\frac{F_0}{\rm erg\ cm^{-2}\ s^{-1}}\right) - \log 4\pi\right]. \quad (2)$$

To calibrate A we shall use the nearest GRBs of our sample: (1) 171205A at $z = 0.0368$, (2) 180728A at $z = 0.117$, and (3) 130702A at $z = 0.145$ and 161219B at $z = 0.1475$, almost at the same distance. In Equation (2) we replace $\mu_{\rm GRB}$ with the average distance modulus $\langle \mu_{\rm SN\ Ia} \rangle$ computed from SNe Ia at the same z of the above four sources (Amanullah et al. 2010; Suzuki et al. 2012), and we use the value of γ from Section 2.2.1 and the values of F_0, $E_{\rm p,i}$, τ, and α for each of the four GRBs from Table 4. We infer: (1) $\langle \mu_{\rm SN\ Ia} \rangle = 35.97 \pm 0.17$ and $\log[A/({\rm erg\ s^{-1}})] = 48.61 \pm 0.42$ for GRB 171205A; (2) $\langle \mu_{\rm SN\ Ia} \rangle = 38.68 \pm 0.09$ and $\log[A/({\rm erg\ s^{-1}})] = 48.97 \pm 0.25$ for GRB 180728A; (3) $\langle \mu_{\rm SN\ Ia} \rangle = 39.21 \pm 0.24$ and $\log[A/({\rm erg\ s^{-1}})] = 49.52 \pm 0.21$ for GRB 130702A and $\log[A/({\rm erg\ s^{-1}})] = 50.09 \pm 1.12$ for GRB 161219B. Indeed, in estimating the normalization, we select the values of A coming from GRBs 130702A and 161219B because they represent a small set of bursts at the same z.[13] Their weighted average value is $\log[A/({\rm erg\ s^{-1}})] = 49.54 \pm 0.21$.

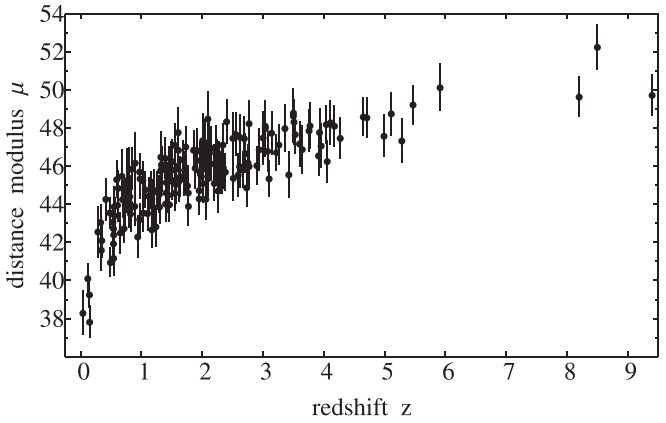

Figure 4. The GRB Hubble diagram of the Combo relation.

Table 1
Best-fit Parameters of the Seven Sub-samples at Average Redshift $\langle z \rangle$: The Slope γ_z, the Normalization A_z, and the Extra-Scatter $\sigma_{{\rm ex},z}$ are Shown

$\langle z \rangle$	γ_z	$\log(A_z/{\rm cm^2\ s^{-1}})$	$\sigma_{{\rm ex},z}$
0.54 ± 0.01	0.81 ± 0.49	-7.38 ± 1.08	0.29 ± 0.10
1.18 ± 0.07	0.83 ± 0.31	-7.93 ± 0.77	0.26 ± 0.08
1.46 ± 0.05	0.80 ± 0.32	-8.29 ± 0.79	0.26 ± 0.08
1.70 ± 0.06	0.94 ± 0.32	-8.92 ± 0.84	0.19 ± 0.08
2.05 ± 0.05	1.05 ± 0.32	-9.44 ± 0.90	0.34 ± 0.08
2.27 ± 0.07	0.78 ± 0.20	-8.57 ± 0.54	0.16 ± 0.06
2.69 ± 0.08	1.02 ± 0.34	-9.38 ± 0.87	0.34 ± 0.10

3. Testing the Standard ΛCDM Model

GRB distance moduli $\mu_{\rm GRB}$ and their uncertainties $\sigma\mu_{\rm GRB}$ (see Figure 4) depend upon the set of observables ($E_{\rm p,i}$, τ, α, F_0) and the relation parameters. They can be compared with the theoretical distance moduli $\mu_{\rm th} = -97.45 + 5\log\{d_l[z, \Omega_m, \Omega_\Lambda, w(z), H_0]/{\rm cm}\}$, where the luminosity distance d_l is defined as (see, e.g., Goobar & Perlmutter 1995)

$$d_l = \frac{c}{H_0}\frac{(1+z)}{\sqrt{|\Omega_k|}} F_k\left(\int_0^z \frac{\sqrt{|\Omega_k|}\, dz'}{\sqrt{E[z', \Omega_m, \Omega_\Lambda, w]}}\right), \quad (3)$$

[13] Single GRB estimates are disfavored because they might be above/below the relation and, thus, over/underestimate the value of A. Small sample estimates in general average these effects.

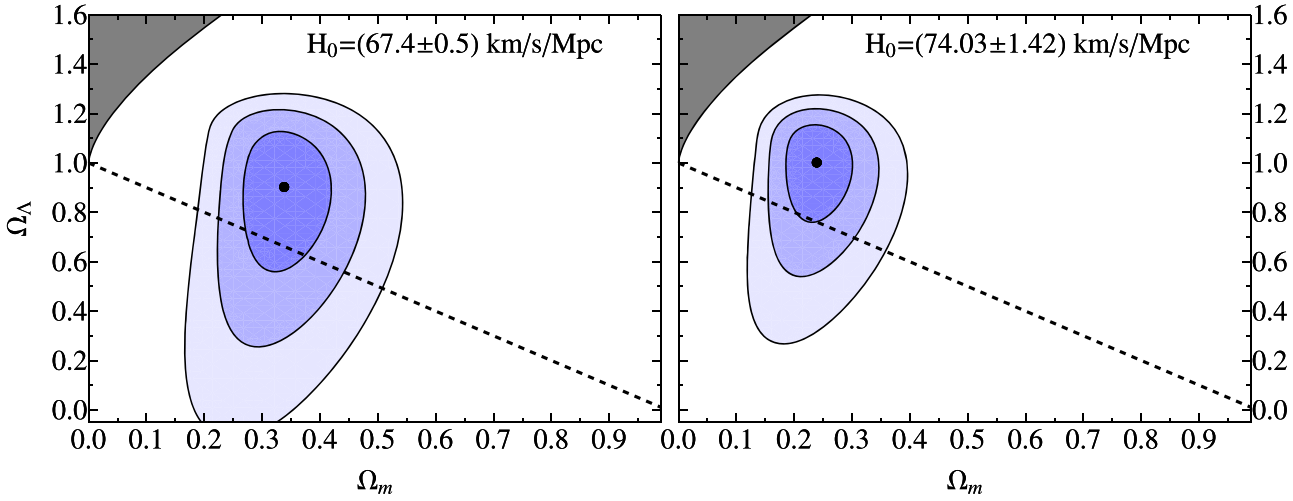

Figure 5. Best-fit parameters (black circles) and confidence regions (1, 2, and 3σ from the inner/darker to the outer/lighter) in the Ω_m–Ω_Λ plane for the selected H_0. The gray regions indicate the set of parameters for which no big bang occurs while the dashed lines are those of a flat universe case.

Table 2
Best-fit Parameters with 1σ Uncertainties for the Various Cosmological Cases Discussed in this Work

H_0	Ω_m	Ω_Λ	Ω_k	w	χ^2
		Flat ΛCDM (DOF = 173)			
P20	$0.32^{+0.05}_{-0.05}$	$0.68^{+0.05}_{-0.05}$	0	−1	165.54
R19	$0.22^{+0.04}_{-0.03}$	$0.78^{+0.04}_{-0.03}$	0	−1	171.32
		ΛCDM (DOF = 172)			
P20	$0.34^{+0.08}_{-0.07}$	$0.91^{+0.22}_{-0.35}$	$-0.24^{+0.24}_{-0.35}$	−1	164.38
R19	$0.24^{+0.06}_{-0.05}$	$1.01^{+0.15}_{-0.25}$	$-0.24^{+0.16}_{-0.25}$	−1	169.23

Note. The last column lists the values of the χ^2. H_0 is fixed to the values given by P20 and R19 (see text).

with $E[z, \Omega_m, \Omega_\Lambda, w] = \Omega_m(1+z)^3 + \Omega_\Lambda(1+z)^{3(1+w)} + \Omega_k(1+z)^2$, $\Omega_k = 1 - \Omega_m - \Omega_\Lambda$, and $F_k(x) = \sinh(x)$ for $\Omega_k > 0$, $F_k(x) = x$ for $\Omega_k = 0$, and $F_k(x) = \sin(x)\}$ for $\Omega_k < 0$.

We first constrain the Hubble constant H_0 with two recent estimates, in tension at 4.4σ: $H_0 = (67.4 \pm 0.5)$ km s^{-1} Mpc^{-1} (P20) and $H_0 = (74.03 \pm 1.42)$ km s^{-1} Mpc^{-1} (Riess et al. 2019, hereafter R19). Then we compare $\mu_{\rm GRB}$ and $\mu_{\rm th}$ distributions and find the best-fit cosmological parameters by performing a χ^2 statistic test.

We first take the flat ΛCDM model and then we leave Ω_k free to vary. In the first case we impose $\Omega_\Lambda = 1 - \Omega_m$ and we summarize our findings in Table 2. In particular, GRBs provide: $\Omega_m = 0.32^{+0.05}_{-0.05}$ for the H_0 of P20 and $\Omega_m = 0.22^{+0.04}_{-0.03}$ for the H_0 of R19, whereas fits using the non-flat ΛCDM model provide large values of $\Omega_{\rm k}$ which are consistent within the errors with the flat ΛCDM case (see Table 2 and Figure 5). Our large and negative value of the curvature parameter is compatible with the recent one obtained by Wei & Melia (2020) using only quasar data calibrated via observational Hubble data set (OHD). However, in Wei & Melia (2020) the best-fit value $\Omega_{\rm k} = -0.918 \pm 0.429$ has a large uncertainty, due to the error propagations induced by anchored OHD, and it is in disagreement with the concordance model at 2.1σ level and at 1.6σ level with respect to our findings.

Worth noticing, the best-fit Ω_m values listed in Table 2, though obtained by using different values of H_0, are consistent with each other.

4. Piecewise Reconstruction of $w(z)$ in Flat Background Cosmology

We consider now a flat universe with an evolving DE EoS. We adopt a redshift-binned parameterization for $w(z)$: a step function with different and constant values of w in each of the redshift bins over which the entire redshift range covered by GRBs is divided (Daly & Djorgovski 2004; King et al. 2014).

The number of bins is arbitrarily defined but holds a set of heuristic assumptions that we made before deciding the redshift interval for each bin. First, we have to notice that the number of bins requires the number of points that is enough to guarantee a suitable interpolation. Second, we expect the number of points increases with the redshifts since most of the GRBs of the sample are located at larger redshifts. This implies that we cannot choose tighter intervals as z increases to include always the same number of data points. Rather than following this strategy, we presume to work at least with 15 points for each bin and to split the intervals in redshift differences of about $\Delta z \sim 0.5$. In so doing, we assume the following four intervals for Δz_i: $\Delta z_1 = 0.55$, $\Delta z_2 = 0.63$, $\Delta z_3 = 0.56$ and $\Delta z_4 = 0.81$, whereas we assume the last interval up to $z \sim 9.5$ since in it we count 48 data points. In this respect the number of data for each interval only slightly increases, leaving unaltered the statistical significance of our fits for each interval. The bins are therefore statistically supported and reported in Table 3.

In Equation (3) we can set

$$E[\Omega_m, f(z_{N-1} < z \leqslant z_N)] = \Omega_m(1+z)^3 + (1-\Omega_m) f(z_{N-1} < z \leqslant z_N), \quad (4)$$

with parametric DE evolution $f(z_{N-1} < z \leqslant z_N)$ given by

$$f(z_{N-1} < z \leqslant z_N) = (1+z)^{3(1+\tilde{w}_N)} \prod_{i=0}^{N-1} \times [1 + \max(z_i)]^{3(\tilde{w}_i - \tilde{w}_{i+1})}, \quad (5)$$

in which N is the redshift bin where z resides and $\tilde{w}_i$ the EoS parameter in the ith redshift bin defined by its maximum

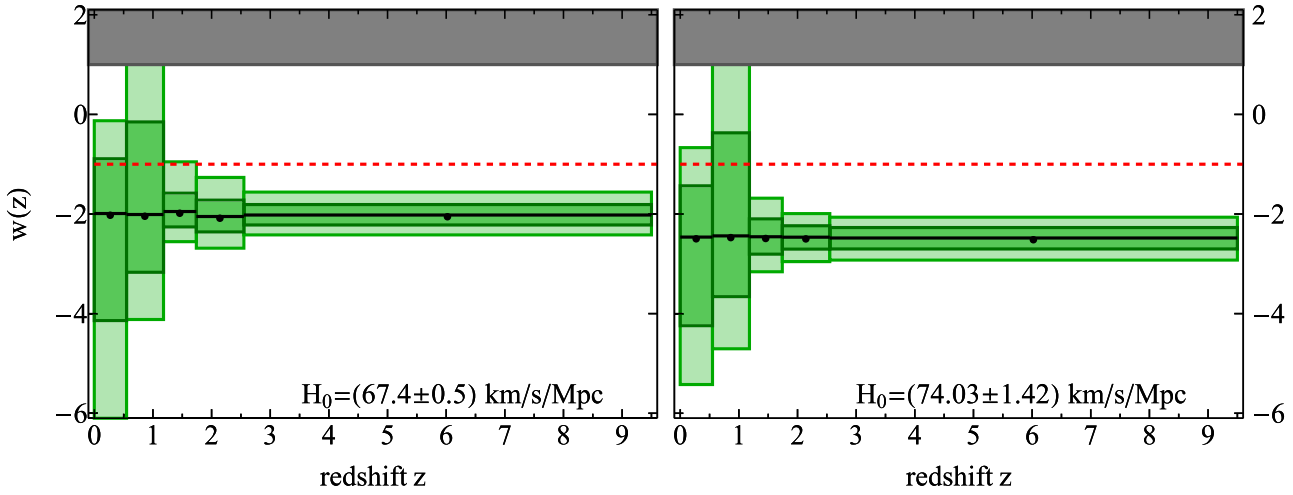

Figure 6. The DE EoS reconstructed evolution through the redshift-binned parameterization of $w(z)$ (1 and 2σ from the inner/darker to the outer/lighter) for the selected H_0. The dashed red lines mark the value $w=-1$ in the flat ΛCDM model. The darker region shows unphysical EoS, i.e., exceeding the stiff matter regime.

Table 3
Upper Part: Redshift Bin z_i, the Number of GRBs N_i within, and the Corresponding Best-fit Uncorrelated w_i (with 1σ Attached Errors) for the H_0 of P20 and R19. Lower part: Values of the χ^2 Over the DOF

z_i	N_i	w_i	
		P20	R19
0.00–0.55	16	$-1.99^{+1.10}_{-2.15}$	$-2.46^{+1.03}_{-1.78}$
0.55–1.18	32	$-2.01^{+1.86}_{-1.16}$	$-2.44^{+2.07}_{-1.22}$
1.18–1.74	35	$-1.95^{+0.37}_{-0.31}$	$-2.46^{+0.36}_{-0.35}$
1.74–2.55	43	$-2.05^{+0.33}_{-0.31}$	$-2.47^{+0.23}_{-0.24}$
2.55–9.50	48	$-2.02^{+0.21}_{-0.20}$	$-2.48^{+0.21}_{-0.22}$
χ^2/DOF		168.02/169	161.12/169

redshift $\max(z_i)$. This parameterization makes no assumptions on DE's nature since different parameters are introduced in every redshift bin. However, the parameters w_i are usually correlated with each other (see Equation (5)). This means that the covariance matrix

$$C = \langle \tilde{w}\tilde{w}^{\mathrm{T}} \rangle - \langle \tilde{w} \rangle \langle \tilde{w}^{\mathrm{T}} \rangle, \tag{6}$$

computed from the vector $\tilde{w}$ with components w_i and the transposed one $\tilde{w}^{\mathrm{T}}$, is not diagonal. Following Huterer & Cooray (2005), to uncorrelate the DE parameters $\tilde{w}_i$ we transform them through an orthogonal matrix rotation O into a basis that diagonalizes the inverse of the covariance matrix, i.e., $\boldsymbol{C}^{-1} = \boldsymbol{O}^{\mathrm{T}}\boldsymbol{\Lambda}\boldsymbol{O}$, where $\boldsymbol{\Lambda}$ is diagonal. The new set of uncorrelated DE parameters w_i is then given by applying a weight matrix defined as $\tilde{W} = O^{\mathrm{T}}\boldsymbol{\Lambda}^{1/2}O$ to the correlated $\tilde{w}_i$. $\tilde{W}$ is normalized in such a way that its rows, the weights for $\tilde{w}_i$, sum to unity.

We first marginalize over the Ω_m parameter using the values inferred for the flat ΛCDM case (see Table 2). Then, we determine five redshift bins to ensure a sufficient number of GRB events for each of them (see Table 3). The average vector $\langle \tilde{w} \rangle$ is calculated by letting $\tilde{w}$ run over the above marginalization over Ω_m. The results of the analysis are summarized in Table 3 and Figure 6. It is worth noting that, for both the values of H_0, the w_i are consistent with the value $w=-1$ for $z \lesssim 1.2$.

5. Theoretical Discussions over w Evolution

Our aim is to use the updated sample of 174 GRBs alone in order to get bounds over DE evolution. Consequently, we obtain tighter constraints on the cosmological parameters, compared to previous results in I15, where a smaller GRB sample has been used. This first result certifies the goodness of our Combo relation compared with other calibration functions, where the increase of data points does not forcedly lead to improving the quality of fits (Luongo & Muccino 2020b).

Moreover, we here investigate the idea of fitting cosmological models with GRBs only, i.e., without considering surveys of standard candles. This procedure resembles the analogous method proposed by Risaliti & Lusso (2019), where the authors investigated how to get constraints in cosmology by using only quasars, although a scaling between the Hubble diagram of quasars with that of SNe in the common redshift range $z=0.1$–1.44 has been applied. Even though GRBs are not genuine standard candles, their use in cosmology leads to promising outcomes and seems to show a particular behavior constraining Ω_m. In particular, from our findings we first conclude that the higher the H_0 value,

1. the lower the best-fit value of Ω_m, and
2. the better the accuracy on cosmological parameters.

However, in all our fits the outcomes have been jeopardized by the common issues related to the use of GRBs in background cosmology (Izzo et al. 2012). A few of these caveats are discussed below in view of our approach.

5.1. Issues with Low-z GRBs

The shortage of very low-z GRBs prevents us from obtaining a precise value of H_0 using GRBs alone. In other words, GRBs alone are unable to fix H_0 and to heal somehow the net tension between recent measurements on it, see e.g., P20 and R19. This is essential for our fits, as if one has a well-bounded H_0 the corresponding findings become stabler, implying that H_0 plays the role of *an initial value* that fixes the shapes of Hubble curves used in the fit (Aviles et al. 2012, 2014; Gruber & Luongo 2014).

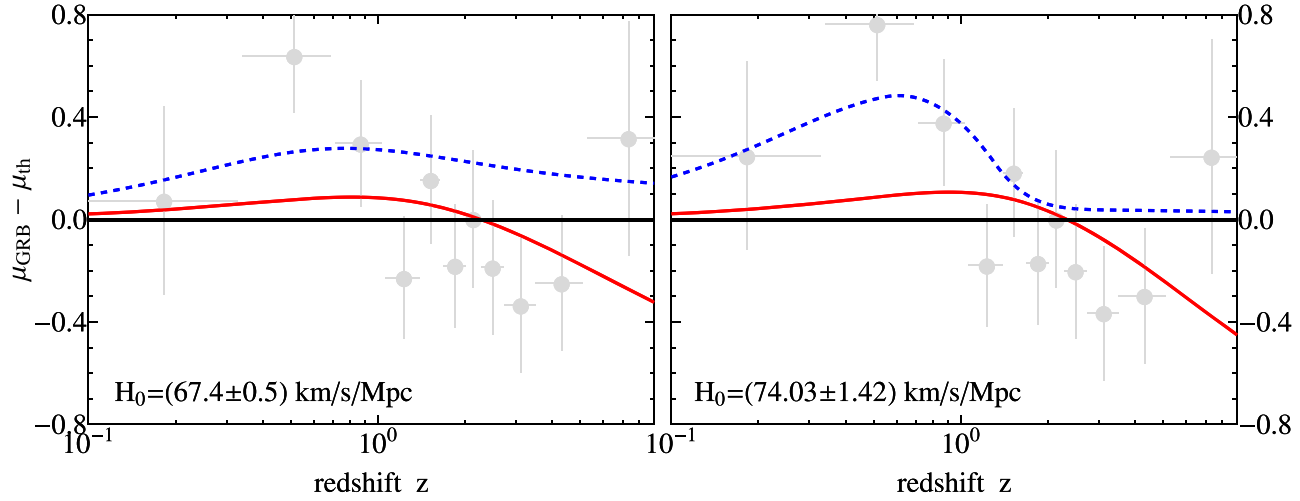

Figure 7. The rebinned GRB moduli μ_{GRB} (gray circles) for the H_0 in P20 and R19 compared with the flat ΛCDM model μ_{th} (see the horizontal black line and Table 2), the non-flat ΛCDM case (see the red line and Table 2), and the flat model with an evolving $w(z)$ (see the dashed blue line and Table 3).

Thus, the lacking of GRBs at small redshift severely acts on our fits. In fact, at $z \simeq 0$ we have no possibility to definitively conclude that the correct cosmological model is the ΛCDM paradigm.

This means that our approach turns out to be more predictive at intermediate redshifts, i.e., as $z > 1.2$. Motivated by this fact, we fixed H_0 in our analyses. To do so, we considered the two most recent measurements of H_0 by P20 and R19 in tension between each other. It is needful to fix the kinematics of our fit for the above reasons, i.e., we do not have enough GRB sources at small redshifts.

Consequently, our findings in the windows of $z < 1.2$ permit us to take the ΛCDM suite but leave open the possibility that DE evolves. Other probes certify slight departures from the case $w = -1$, suggesting that our wide window found using GRBs only at $z = 0$ is only due to the lack of sources in this regime.

Going further with the redshift, i.e., as $z > 1.2$, leads to refined limits over the DE evolution as we discuss below. Precisely, concerning the redshift-evolving DE EoS, we find that at redshift $z \lesssim 1.2$ the evolution of w is almost consistent with the cosmological constant case within 1σ for both the H_0 of R19 and P20.

5.2. Dark Energy Evolution at High z

A first evident deviation from the above-discussed case arises at $z \gtrsim 1.5$, where departures from the ΛCDM case lie on $\gtrsim 2.4\sigma$ for the H_0 of P20 and on $\gtrsim 4\sigma$ for the H_0 of R19. Clearly, at $z \gtrsim 1.5$ a severe observational bias exists and we could indeed observe only the brightest GRBs (Bryant et al. 2020).[14]

It is evident that the shortage of GRBs at low redshifts has a strong influence for the estimate of the DE EoS parameters w. Indeed, DE has its large effects in the low-z universe ($z \lesssim 0.5$), where ≈9% of the Combo-GRBs are located. Moreover, while at low-z the DE drives the evolution of the universe, at $z \geqslant 1$ the matter dominates. In this light, the epoch of the transition between a DE and a matter-dominated universe can represent a new constrain for cosmological models (L. Izzo et al. 2021, in preparation).

The Combo-GRB sample and analysis confirm a universe dominated by DE at low redshifts, but seems to show a fraction of DE to act even at higher redshifts. Although our data analysis within the flat ΛCDM model is in agreement with other recent results from different probes (e.g., P20 and R19), our results prompt a strongly negative mean value for the evolving EoS at intermediate z.

In this case, DE may exhibit a phantom behavior, being a likely though troublesome DE candidate. In particular, at larger z current data do not allow excluding that $w(z)$ might vary with the redshift, possibly to values $w \lesssim -1$. This finding is somehow in line with recent results from Risaliti & Lusso (2019), supporting values of the DE parameter $w < -1$, i.e., a DE density increasing with time, for $z \gtrsim 1.4$.[15] Phrasing it differently, we find that the cosmological evolution is driven by DE in lieu of a pure Λ. By construction the term that dominates is, however, strongly negative, i.e., its evolution shows $w < -1$. As a desirable consequence of this scenario, such a consideration leads to a universe that begins at Big-Bang and terminates at Big-Rip (Caldwell 2002). Indeed, if phantom energy continues driving the universe outward, it could literally tear space into shreds, leading to an unavoidable big rip, as pointed out in Caldwell et al. (2003).

Although appealing, this scenario is unlikely and turns out to be misleading for essentially two main reasons. First, the ΛCDM model lies inside our predictions, within the 1σ. Hence, the simplest framework is clearly favored over any deviations. Second, it is arguable that a phantom DE is disfavored and the fact that DE stabilizes its evolution as z increases indicates the need of refined initial values, as stated above. In other words, although the Combo relation improves the quality of overall analyses with GRBs, the lack of such sources at small redshifts influences the analysis as $z > 1.2$.

Summing up, the cosmological constant model is still inside the GRBs predictions obtained from the use of the Combo relation. Evident deviations to phantom DE and/or to slight

[14] Further analysis on this aspect, including the systematics on the entire sample, will be discussed elsewhere.

[15] For the inconsistency of the quasar data with the ΛCDM model, i.e., $w = -1$, see also Yang et al. (2020) and Velten & Gomes (2020).

variation from $w=-1$ may be addressed noticing that at $z\simeq 0$ not enough GRB sources are available.

5.3. Does the Cosmic Speed up Behave Like Phantom?

The overall fitting procedures that we considered are clearly dependent on the choice of the data sets and bins here used. In particular, using GRBs alone likely leads to $w<-1$, while adopting combined data sets would significantly help to refine the numerical outcomes. However, when involving more than one data set based on GRBs, although it provides consistency with P20, the errors are suitably large, with significant discrepancy. The case is similar to that found for quasars, since, treated separately, there is no tension, but as one attempts to anchor them using another distance indicator (Wei & Melia 2020), one gets issues on errors. Thus, the indication $w<-1$ provided by GRBs can be refined but with further error propagations induced by anchored further data surveys. A relevant approach to overcome this issue is to enlarge the whole data set adopting alternative strategies of experimental analysis (see, e.g., Luongo & Muccino 2020b).

6. Final Remarks

In this work, we considered an extended GRB sample, characterized by 174 GRBs and we fixed limits over DE's evolution using the Combo relation. We extended the approach made in I15 and we got refined bounds over the whole matter content, i.e., Ω_m and DE density. We first worked with the ΛCDM model and then we constrained the evolution of $w(z)$ through a piecewise formulation over seven GRB redshift interval bins. We theoretically discussed our results, showing an overall agreement with the ΛCDM model that lies inside our findings. We distinguished two regimes, $z<1.2$ and $z\geqslant 1.2$, where GRBs turn out to be more predictive. Deviations from $w=-1$ are not excluded in both the intervals. However, we proposed that at small redshifts, deviations from $w=-1$ are jeopardized by the GRB shortage. As the redshift increases, DE's abundance is much more constrained with GRBs. Thus, beyond $z\simeq 1.2$ the case $w<-1$ cannot be fully excluded from our computations.

In particular, a concise summary of the fitting of $\mu_{\rm GRB}$ with various cosmological models has been shown in Figure 7, where we compared the residual GRB distance moduli $\mu_{\rm GRB}$ with respect the $\mu_{\rm th}$ from the flat ΛCDM case (see horizontal black line and Table 2). In Figure 7 we also compared these figures with the distance moduli from the non-flat ΛCDM case (see the red line and Table 2), and the flat wCDM with an evolving $w(z)$ (see the dashed blue line and Table 3).

From all our analyses we obtained the following main results:

(1) the Combo-GRB sample confirmed a DE-dominated universe, responsible for the observed acceleration at low redshifts. Our data analysis within the flat ΛCDM model is in agreement with other recent results from different probes (e.g., P20 and R19);
(2) as stated above, it was clear that the shortage of GRBs at low redshifts has a strong influence for the estimate of w. This happens since DE has its large effects around $z\lesssim 0.5$, where $\approx$9% of the Combo-GRBs are located;
(3) the value of $w(z)$ agreed, within 1σ, with the standard ΛCDM model up to $z\approx 1.2$. At larger z, current data do not allow excluding that $w(z)$ might vary with the redshift, possibly to values $w\lesssim -1$. This finding is somehow in line with recent results from Risaliti & Lusso (2019), supporting values of the DE parameter $w<-1$, i.e., a DE density increasing with time, for $z\gtrsim 1.4$.

From the above considerations, we concluded by remarking the important role of GRBs as probes for the low- and high-z universe: the evidence of tight correlations between their observed properties has really become crucial to understanding the evolution history of the universe at very large redshifts, where no astrophysical probe has gone before.

Future perspectives are based on missions like the incoming SVOM and the proposed eXTP and THESEUS that will provide a robust data set of GRBs at all redshifts ($\approx$100 at $z\gtrsim 5$ over a three year mission) allowing a more detailed study of the early universe up the re-ionization era. The application of this forthcoming data set to further test the Combo relation can also shed light on the physics of the X-ray afterglow and provide a physical explanation behind this GRB relation (see, e.g., Muccino & Boshkayev 2017; Stratta et al. 2018).

The authors are thankful to the anonymous referee for constructive suggestions that helped to significantly improve the manuscript. This work made use of data supplied by the UK Swift Science Data Center at the University of Leicester. K.B. is supported by the Ministry of Education and Science of the Republic of Kazakhstan, Grant: IRN AP08052311. M.M. is supported by INFN as part of the MoonLIGHT-2 experiment in the framework of the research activities of Commissione Scientifica Nazionale 2. L.A. acknowledges financial contribution from the agreement ASI-INAF n. 2017-14-H.O. We warmly thank Michael Oliver for the support in completing this paper.

Appendix
The Sample

In Table 4 we list the full sample long GRBs used in this work and their Combo relation parameters.

Table 4
List of the Long Bursts Analyzed in I15 and in this Work (in Boldface) and their Combo Relation Parameters

GRB	z	Sub-sample	$\log(E_{\rm p,i}/{\rm keV})$	$\log(F_0/{\rm erg\ cm^{-2}\ s})$	$\log(\tau/{\rm s})$	α
050401	2.8983		$2.67^{+0.13}_{-0.11}$	$-9.57^{+0.02}_{-0.02}$	$2.90^{+0.06}_{-0.07}$	-1.75 ± 0.09
050922C	2.1995	*f*	$2.62^{+0.13}_{-0.10}$	$-8.79^{+0.05}_{-0.06}$	$1.64^{+0.07}_{-0.09}$	-1.30 ± 0.03
051109A	2.346		$2.73^{+0.13}_{-0.19}$	$-9.86^{+0.07}_{-0.09}$	$2.97^{+0.08}_{-0.10}$	-1.36 ± 0.03
060115	3.53		$2.47^{+0.05}_{-0.05}$	$-11.15^{+0.06}_{-0.06}$	$3.99^{+0.13}_{-0.19}$	-2.64 ± 0.44
060418	1.489	*c*	$2.76^{+0.10}_{-0.12}$	$-9.22^{+0.07}_{-0.08}$	$2.49^{+0.08}_{-0.10}$	-1.64 ± 0.06
060526	3.2213		$2.02^{+0.08}_{-0.10}$	$-11.31^{+0.04}_{-0.04}$	$4.53^{+0.14}_{-0.21}$	-5.23 ± 1.40
060707	3.424		$2.44^{+0.13}_{-0.08}$	$-10.60^{+0.14}_{-0.21}$	$2.87^{+0.19}_{-0.36}$	-1.07 ± 0.05
060729	0.54	*a*	$1.89^{+0.12}_{-0.16}$	$-10.54^{+0.01}_{-0.01}$	$4.80^{+0.02}_{-0.02}$	-1.76 ± 0.03

Table 4
(Continued)

GRB	z	Sub-sample	$\log(E_{\rm p,i}/{\rm keV})$	$\log(F_0/{\rm erg\ cm^{-2}\ s})$	$\log(\tau/{\rm s})$	α
060814	0.84		$2.88^{+0.12}_{-0.17}$	$-10.42^{+0.04}_{-0.04}$	$3.88^{+0.06}_{-0.07}$	-1.56 ± 0.07
060908	1.8836	*d*	$2.74^{+0.07}_{-0.09}$	$-8.50^{+0.07}_{-0.08}$	$1.65^{+0.10}_{-0.13}$	-1.37 ± 0.05
060927	5.467		$2.44^{+0.10}_{-0.14}$	$-10.80^{+0.06}_{-0.06}$	$2.51^{+0.11}_{-0.15}$	-1.55 ± 0.17
061121	1.3145		$3.11^{+0.05}_{-0.05}$	$-9.52^{+0.01}_{-0.01}$	$3.23^{+0.02}_{-0.02}$	-1.55 ± 0.02
071020	2.1462		$3.01^{+0.06}_{-0.07}$	$-8.50^{+0.06}_{-0.07}$	$1.22^{+0.07}_{-0.09}$	-1.21 ± 0.02
080319B	0.9382		$3.10^{+0.01}_{-0.01}$	$-6.13^{+0.03}_{-0.03}$	$1.29^{+0.03}_{-0.03}$	-1.67 ± 0.01
080413B	1.1014	*b*	$2.21^{+0.05}_{-0.06}$	$-9.15^{+0.04}_{-0.04}$	$1.97^{+0.06}_{-0.07}$	-1.06 ± 0.02
080605	1.6403	*d*	$2.88^{+0.04}_{-0.05}$	$-8.45^{+0.02}_{-0.02}$	$1.94^{+0.03}_{-0.03}$	-1.41 ± 0.02
080607	3.0368		$3.23^{+0.05}_{-0.04}$	$-9.72^{+0.08}_{-0.09}$	$2.73^{+0.08}_{-0.10}$	-1.76 ± 0.07
080721	2.5914		$3.24^{+0.06}_{-0.06}$	$-8.11^{+0.01}_{-0.01}$	$1.97^{+0.01}_{-0.01}$	-1.48 ± 0.01
080810	3.3604		$3.17^{+0.05}_{-0.06}$	$-9.71^{+0.13}_{-0.18}$	$2.86^{+0.13}_{-0.19}$	-2.07 ± 0.15
080916A	0.689		$2.32^{+0.04}_{-0.05}$	$-10.32^{+0.06}_{-0.07}$	$3.09^{+0.10}_{-0.12}$	-1.08 ± 0.04
080928	1.692	*d*	$1.98^{+0.09}_{-0.12}$	$-10.27^{+0.06}_{-0.07}$	$3.60^{+0.09}_{-0.11}$	-2.66 ± 0.21
081007	0.5295	*a*	$1.79^{+0.10}_{-0.12}$	$-10.19^{+0.05}_{-0.05}$	$3.20^{+0.07}_{-0.09}$	-1.15 ± 0.04
081008	1.9685	*d*	$2.42^{+0.08}_{-0.10}$	$-10.15^{+0.04}_{-0.04}$	$3.23^{+0.07}_{-0.08}$	-1.93 ± 0.11
081222	2.77	*g*	$2.80^{+0.04}_{-0.05}$	$-8.52^{+0.03}_{-0.03}$	$1.45^{+0.04}_{-0.04}$	-1.22 ± 0.01
090102	1.547		$3.07^{+0.04}_{-0.05}$	$-8.38^{+0.09}_{-0.11}$	$1.93^{+0.09}_{-0.11}$	-1.45 ± 0.03
090418A	1.608		$3.20^{+0.10}_{-0.12}$	$-9.34^{+0.02}_{-0.02}$	$2.78^{+0.04}_{-0.05}$	-1.68 ± 0.05
090423	8.2		$2.65^{+0.05}_{-0.05}$	$-11.25^{+0.06}_{-0.06}$	$2.68^{+0.12}_{-0.17}$	-1.28 ± 0.14
090424	0.544	*a*	$2.40^{+0.04}_{-0.05}$	$-8.39^{+0.03}_{-0.03}$	$2.39^{+0.03}_{-0.04}$	-1.21 ± 0.01
090516	4.109		$2.99^{+0.18}_{-0.11}$	$-10.49^{+0.05}_{-0.06}$	$3.40^{+0.08}_{-0.09}$	-2.20 ± 0.14
090618	0.54	*a*	$2.40^{+0.04}_{-0.05}$	$-8.89^{+0.01}_{-0.01}$	$3.06^{+0.02}_{-0.02}$	-1.44 ± 0.01
091018	0.971		$1.74^{+0.13}_{-0.20}$	$-9.03^{+0.02}_{-0.03}$	$2.24^{+0.04}_{-0.05}$	-1.29 ± 0.02
091020	1.71	*d*	$2.71^{+0.05}_{-0.06}$	$-9.29^{+0.03}_{-0.03}$	$2.40^{+0.04}_{-0.05}$	-1.34 ± 0.03
091029	2.752	*g*	$2.36^{+0.11}_{-0.15}$	$-10.85^{+0.02}_{-0.03}$	$3.57^{+0.05}_{-0.06}$	-1.39 ± 0.05
091127	0.49		$1.71^{+0.04}_{-0.05}$	$-8.99^{+0.03}_{-0.03}$	$3.33^{+0.03}_{-0.04}$	-1.52 ± 0.02
100621A	0.542	*a*	$2.16^{+0.08}_{-0.06}$	$-9.77^{+0.05}_{-0.06}$	$3.62^{+0.08}_{-0.10}$	-1.08 ± 0.04
100814A	1.44	*c*	$2.41^{+0.05}_{-0.06}$	$-10.76^{+0.01}_{-0.02}$	$4.85^{+0.05}_{-0.05}$	-2.77 ± 0.16
100906A	1.727	*d*	$2.46^{+0.06}_{-0.08}$	$-9.83^{+0.04}_{-0.04}$	$3.40^{+0.05}_{-0.06}$	-2.27 ± 0.10
110213A	1.46	*c*	$2.35^{+0.04}_{-0.04}$	$-9.23^{+0.02}_{-0.02}$	$3.39^{+0.04}_{-0.04}$	-2.48 ± 0.09
110422A	1.77		$2.62^{+0.01}_{-0.01}$	$-8.63^{+0.08}_{-0.10}$	$2.13^{+0.09}_{-0.12}$	-1.33 ± 0.03
111228A	0.714		$1.76^{+0.05}_{-0.06}$	$-10.10^{+0.03}_{-0.03}$	$3.68^{+0.05}_{-0.06}$	-1.42 ± 0.04
120119A	1.728	*d*	$2.70^{+0.04}_{-0.05}$	$-10.61^{+0.08}_{-0.10}$	$3.69^{+0.13}_{-0.19}$	-1.99 ± 0.23
120811C	2.671	*g*	$2.30^{+0.02}_{-0.02}$	$-10.16^{+0.04}_{-0.04}$	$3.12^{+0.12}_{-0.16}$	-1.57 ± 0.18
120907A	0.97		$2.48^{+0.08}_{-0.10}$	$-10.11^{+0.04}_{-0.05}$	$2.75^{+0.07}_{-0.09}$	-1.17 ± 0.04
120922A	3.1		$2.19^{+0.04}_{-0.04}$	$-9.81^{+0.09}_{-0.11}$	$2.26^{+0.11}_{-0.15}$	-1.14 ± 0.04
121128A	2.2	*f*	$2.39^{+0.02}_{-0.02}$	$-9.16^{+0.03}_{-0.04}$	$2.84^{+0.07}_{-0.08}$	-2.27 ± 0.14
121211A	1.023		$2.29^{+0.05}_{-0.06}$	$-10.57^{+0.08}_{-0.09}$	$3.41^{+0.14}_{-0.20}$	-1.27 ± 0.11
130408A	3.757		$3.00^{+0.06}_{-0.07}$	$-9.96^{+0.05}_{-0.05}$	$2.81^{+0.08}_{-0.10}$	-1.66 ± 0.12
130420A	1.297		$2.11^{+0.02}_{-0.02}$	$-10.25^{+0.06}_{-0.07}$	$2.76^{+0.10}_{-0.13}$	-1.05 ± 0.03
130427A	0.3399		$3.06^{+0.01}_{-0.01}$	$-7.63^{+0.02}_{-0.02}$	$2.79^{+0.03}_{-0.03}$	-1.37 ± 0.01
130505A	2.27	*f*	$3.31^{+0.02}_{-0.02}$	$-9.30^{+0.04}_{-0.04}$	$3.24^{+0.04}_{-0.05}$	-1.65 ± 0.03
130610A	2.092	*e*	$2.96^{+0.06}_{-0.07}$	$-9.71^{+0.24}_{-0.56}$	$1.81^{+0.20}_{-0.37}$	-1.23 ± 0.12
130612A	2.006	*e*	$2.27^{+0.07}_{-0.08}$	$-10.89^{+0.25}_{-0.65}$	$2.80^{+0.22}_{-0.48}$	-1.22 ± 0.42
130701A	1.155	*b*	$2.28^{+0.02}_{-0.02}$	$-8.60^{+0.10}_{-0.12}$	$1.65^{+0.12}_{-0.16}$	-1.26 ± 0.03
130702A	0.145		$1.17^{+0.06}_{-0.07}$	$-10.44^{+0.05}_{-0.06}$	$4.82^{+0.06}_{-0.08}$	-1.37 ± 0.03
130831A	0.4791		$1.91^{+0.03}_{-0.03}$	$-9.62^{+0.05}_{-0.06}$	$3.25^{+0.06}_{-0.07}$	-1.74 ± 0.07
131030A	1.295		$2.61^{+0.02}_{-0.02}$	$-9.12^{+0.03}_{-0.03}$	$2.60^{+0.05}_{-0.06}$	-1.30 ± 0.02
131105A	1.686	*d*	$2.62^{+0.09}_{-0.12}$	$-10.42^{+0.03}_{-0.04}$	$3.15^{+0.08}_{-0.10}$	-1.28 ± 0.08
131117A	4.042		$2.35^{+0.07}_{-0.08}$	$-10.61^{+0.08}_{-0.10}$	$2.39^{+0.13}_{-0.19}$	-1.30 ± 0.09
140206	2.73	*g*	$2.65^{+0.02}_{-0.02}$	$-9.37^{+0.02}_{-0.02}$	$2.91^{+0.03}_{-0.03}$	-1.44 ± 0.02
140213	1.2076	*b*	$2.25^{+0.01}_{-0.01}$	$-9.76^{+0.04}_{-0.05}$	$3.40^{+0.06}_{-0.07}$	-1.48 ± 0.05
050215B	2.62	*g*	$1.80^{+0.13}_{-0.07}$	$-11.79^{+0.15}_{-0.24}$	$3.47^{+0.23}_{-0.52}$	-1.40 ± 0.28
050315	1.95		$1.95^{+0.08}_{-0.10}$	$-11.05^{+0.02}_{-0.03}$	$4.45^{+0.08}_{-0.10}$	-1.78 ± 0.17
050318	1.4436	*c*	$2.06^{+0.09}_{-0.11}$	$-10.05^{+0.09}_{-0.11}$	$3.31^{+0.12}_{-0.16}$	-2.07 ± 0.18
050505	4.27		$2.79^{+0.13}_{-0.18}$	$-10.53^{+0.03}_{-0.03}$	$3.52^{+0.06}_{-0.07}$	-1.99 ± 0.10
050525A	0.606		$2.11^{+0.04}_{-0.05}$	$-9.26^{+0.05}_{-0.06}$	$2.78^{+0.06}_{-0.07}$	-1.54 ± 0.05
050819A	2.5043		$1.89^{+0.30}_{-0.64}$	$-11.94^{+0.14}_{-0.21}$	$3.62^{+0.26}_{-0.71}$	-1.32 ± 0.29

Table 4
(Continued)

GRB	z	Sub-sample	$\log(E_{\rm p,i}/{\rm keV})$	$\log(F_0/{\rm erg\ cm^{-2}\ s})$	$\log(\tau/{\rm s})$	α
050820A	2.6147	*g*	$3.12^{+0.08}_{-0.10}$	$-9.71^{+0.02}_{-0.02}$	$3.05^{+0.03}_{-0.03}$	-1.28 ± 0.02
051008	2.77	*g*	$3.06^{+0.13}_{-0.18}$	$-10.60^{+0.03}_{-0.03}$	$4.22^{+0.12}_{-0.16}$	-6.02 ± 1.32
051022	0.809		$2.88^{+0.13}_{-0.18}$	$-9.70^{+0.07}_{-0.08}$	$4.12^{+0.07}_{-0.09}$	-2.35 ± 0.11
060111A	2.32	*f*	$2.39^{+0.10}_{-0.06}$	$-11.27^{+0.12}_{-0.17}$	$3.22^{+0.19}_{-0.33}$	-1.04 ± 0.07
060124	2.296	*f*	$2.89^{+0.13}_{-0.20}$	$-9.99^{+0.03}_{-0.04}$	$3.49^{+0.05}_{-0.05}$	-1.49 ± 0.04
060204B	2.3393	*f*	$2.54^{+0.13}_{-0.08}$	$-10.50^{+0.11}_{-0.15}$	$3.21^{+0.16}_{-0.24}$	-1.64 ± 0.14
060206	4.0559		$2.61^{+0.16}_{-0.26}$	$-10.32^{+0.07}_{-0.08}$	$3.33^{+0.09}_{-0.11}$	-1.50 ± 0.05
060210	3.9122		$2.76^{+0.12}_{-0.17}$	$-10.29^{+0.04}_{-0.04}$	$3.39^{+0.06}_{-0.07}$	-1.59 ± 0.06
060306	1.5591		$2.25^{+0.15}_{-0.24}$	$-10.35^{+0.04}_{-0.04}$	$3.10^{+0.07}_{-0.09}$	-1.23 ± 0.05
060319	1.172	*b*	$1.79^{+0.11}_{-0.15}$	$-10.01^{+0.09}_{-0.12}$	$2.41^{+0.12}_{-0.17}$	-1.03 ± 0.02
060502A	1.51		$2.67^{+0.18}_{-0.31}$	$-10.69^{+0.04}_{-0.04}$	$3.61^{+0.08}_{-0.10}$	-1.35 ± 0.06
060512	2.1	*e*	$1.85^{+0.25}_{-0.19}$	$-10.90^{+0.20}_{-0.40}$	$2.98^{+0.24}_{-0.56}$	-1.45 ± 0.17
060522	5.11		$2.69^{+0.20}_{-0.07}$	$-9.71^{+0.08}_{-0.10}$	$1.85^{+0.13}_{-0.19}$	-1.57 ± 0.10
060604	2.1357		$2.10^{+0.05}_{-0.06}$	$-11.13^{+0.06}_{-0.07}$	$3.62^{+0.11}_{-0.14}$	-1.39 ± 0.09
060605	3.773		$2.69^{+0.18}_{-0.33}$	$-10.61^{+0.04}_{-0.04}$	$3.93^{+0.16}_{-0.25}$	-5.82 ± 1.79
060607A	3.0749		$2.68^{+0.10}_{-0.12}$	$-9.74^{+0.04}_{-0.05}$	$3.05^{+0.10}_{-0.14}$	-2.42 ± 0.21
060708	1.92		$2.47^{+0.32}_{-0.06}$	$-10.36^{+0.08}_{-0.10}$	$2.76^{+0.10}_{-0.12}$	-1.27 ± 0.04
060714	2.7108	*g*	$2.37^{+0.16}_{-0.27}$	$-10.40^{+0.04}_{-0.04}$	$3.01^{+0.07}_{-0.09}$	-1.47 ± 0.06
060904A	2.55		$2.76^{+0.08}_{-0.09}$	$-10.56^{+0.06}_{-0.08}$	$3.01^{+0.16}_{-0.26}$	-1.37 ± 0.11
061126	1.159		$3.13^{+0.12}_{-0.16}$	$-8.50^{+0.10}_{-0.14}$	$2.19^{+0.10}_{-0.12}$	-1.37 ± 0.02
061222A	2.088	*e*	$2.94^{+0.07}_{-0.08}$	$-9.49^{+0.03}_{-0.03}$	$3.00^{+0.04}_{-0.04}$	-1.38 ± 0.02
070125	1.547		$2.97^{+0.06}_{-0.07}$	$-11.11^{+0.08}_{-0.09}$	$4.62^{+0.12}_{-0.17}$	-2.65 ± 0.33
070328	2.0627	*e*	$3.18^{+0.13}_{-0.12}$	$-8.37^{+0.01}_{-0.01}$	$2.15^{+0.02}_{-0.02}$	-1.61 ± 0.02
070508	0.82		$2.53^{+0.02}_{-0.02}$	$-8.52^{+0.01}_{-0.01}$	$2.42^{+0.02}_{-0.02}$	-1.46 ± 0.02
070521	2.0865	*e*	$2.84^{+0.05}_{-0.04}$	$-9.49^{+0.04}_{-0.05}$	$2.70^{+0.07}_{-0.09}$	-1.55 ± 0.09
071003	1.6044		$3.31^{+0.04}_{-0.04}$	$-10.53^{+0.13}_{-0.18}$	$3.94^{+0.15}_{-0.22}$	-2.18 ± 0.19
071031	2.6918	*g*	$1.95^{+0.11}_{-0.15}$	$-11.61^{+0.13}_{-0.20}$	$3.67^{+0.22}_{-0.46}$	-1.68 ± 0.33
071117	1.331		$2.05^{+0.18}_{-0.30}$	$-10.64^{+0.11}_{-0.15}$	$3.40^{+0.20}_{-0.38}$	-1.62 ± 0.29
080319C	1.95		$2.96^{+0.11}_{-0.16}$	$-8.61^{+0.04}_{-0.04}$	$2.68^{+0.07}_{-0.08}$	-1.68 ± 0.06
080411	1.0301		$2.72^{+0.06}_{-0.05}$	$-9.19^{+0.04}_{-0.05}$	$3.30^{+0.04}_{-0.05}$	-1.41 ± 0.01
081028	3.038		$2.37^{+0.15}_{-0.22}$	$-12.01^{+0.19}_{-0.35}$	$4.33^{+0.26}_{-0.79}$	-1.83 ± 0.49
081109	0.9787		$2.68^{+0.10}_{-0.12}$	$-9.31^{+0.09}_{-0.12}$	$2.27^{+0.11}_{-0.15}$	-1.17 ± 0.03
081121	2.512		$2.78^{+0.04}_{-0.05}$	$-8.88^{+0.16}_{-0.24}$	$2.41^{+0.14}_{-0.20}$	-1.50 ± 0.03
081203A	2.05	*e*	$3.19^{+0.25}_{-0.15}$	$-9.15^{+0.03}_{-0.03}$	$2.52^{+0.05}_{-0.05}$	-1.85 ± 0.06
081221	2.26	*f*	$2.45^{+0.04}_{-0.05}$	$-8.47^{+0.15}_{-0.24}$	$1.77^{+0.17}_{-0.29}$	-1.32 ± 0.05
090205	4.6497		$2.33^{+0.13}_{-0.18}$	$-10.97^{+0.03}_{-0.04}$	$3.31^{+0.10}_{-0.13}$	-2.63 ± 0.33
090429B	9.4		$2.64^{+0.05}_{-0.06}$	$-10.89^{+0.06}_{-0.07}$	$2.51^{+0.15}_{-0.23}$	-1.46 ± 0.20
090715B	3.0		$2.73^{+0.12}_{-0.17}$	$-10.11^{+0.20}_{-0.40}$	$2.56^{+0.21}_{-0.40}$	-1.33 ± 0.05
090926A	2.1062	*e*	$2.95^{+0.04}_{-0.05}$	$-10.47^{+0.26}_{-0.77}$	$3.71^{+0.24}_{-0.61}$	-1.66 ± 0.12
091003	0.8969		$2.91^{+0.08}_{-0.09}$	$-10.69^{+0.25}_{-0.62}$	$4.06^{+0.25}_{-0.66}$	-1.56 ± 0.14
091208B	1.063		$2.39^{+0.04}_{-0.05}$	$-9.63^{+0.05}_{-0.05}$	$2.49^{+0.07}_{-0.09}$	-1.14 ± 0.03
100728A	1.567		$2.92^{+0.04}_{-0.05}$	$-8.96^{+0.04}_{-0.04}$	$2.78^{+0.05}_{-0.06}$	-1.56 ± 0.04
100728B	2.106	*e*	$2.51^{+0.06}_{-0.07}$	$-9.34^{+0.11}_{-0.14}$	$1.58^{+0.17}_{-0.29}$	-1.17 ± 0.07
101213A	0.414		$2.64^{+0.15}_{-0.23}$	$-10.23^{+0.05}_{-0.06}$	$4.04^{+0.11}_{-0.14}$	-1.47 ± 0.11
101219B	0.5519	*a*	$2.03^{+0.05}_{-0.05}$	$-11.94^{+0.08}_{-0.09}$	$4.48^{+0.19}_{-0.34}$	-1.06 ± 0.17
110106B	0.618		$2.29^{+0.03}_{-0.02}$	$-10.23^{+0.04}_{-0.04}$	$3.41^{+0.08}_{-0.09}$	-1.39 ± 0.06
110205A	2.22	*f*	$2.85^{+0.12}_{-0.18}$	$-9.24^{+0.24}_{-0.55}$	$2.43^{+0.19}_{-0.36}$	-1.67 ± 0.06
110503A	1.613		$2.74^{+0.04}_{-0.05}$	$-8.38^{+0.05}_{-0.06}$	$1.50^{+0.06}_{-0.07}$	-1.18 ± 0.01
110715A	0.82		$2.34^{+0.04}_{-0.05}$	$-8.57^{+0.03}_{-0.03}$	$2.10^{+0.05}_{-0.06}$	-1.23 ± 0.03
110801A	1.858		$2.60^{+0.13}_{-0.19}$	$-10.41^{+0.06}_{-0.06}$	$3.62^{+0.10}_{-0.12}$	-2.38 ± 0.24
111008A	4.9898		$2.95^{+0.10}_{-0.14}$	$-10.19^{+0.03}_{-0.04}$	$3.14^{+0.05}_{-0.05}$	-1.72 ± 0.05
111209A	0.677		$2.72^{+0.07}_{-0.08}$	$-10.96^{+0.19}_{-0.34}$	$4.32^{+0.23}_{-0.54}$	-1.44 ± 0.16
120422A	0.283		$1.52^{+0.34}_{-0.34}$	$-12.35^{+0.06}_{-0.07}$	$4.89^{+0.23}_{-0.51}$	-1.05 ± 0.26
120712A	4.1745		$2.81^{+0.08}_{-0.10}$	$-9.70^{+0.05}_{-0.06}$	$1.97^{+0.10}_{-0.13}$	-1.33 ± 0.07
120729A	0.8		$2.32^{+0.66}_{-0.16}$	$-9.32^{+0.11}_{-0.15}$	$3.13^{+0.06}_{-0.07}$	-2.63 ± 0.15
120909A	3.93		$3.11^{+0.14}_{-0.21}$	$-10.27^{+0.09}_{-0.11}$	$3.09^{+0.13}_{-0.18}$	-1.46 ± 0.12
120923A	8.5		$2.58^{+0.09}_{-0.12}$	$-11.34^{+0.10}_{-0.13}$	$2.00^{+0.19}_{-0.36}$	-1.61 ± 0.21
121027A	1.773		$2.12^{+0.21}_{-0.19}$	$-11.01^{+0.06}_{-0.07}$	$4.48^{+0.11}_{-0.15}$	-1.45 ± 0.11

Table 4
(Continued)

GRB	z	Sub-sample	$\log(E_{\rm p,i}/{\rm keV})$	$\log(F_0/{\rm erg\ cm^{-2}\ s})$	$\log(\tau/{\rm s})$	α
130514A	3.6		$2.70^{+0.11}_{-0.15}$	$-10.68^{+0.10}_{-0.12}$	$3.31^{+0.17}_{-0.28}$	-1.40 ± 0.16
130528A	1.25	*b*	$2.47^{+0.02}_{-0.02}$	$-9.91^{+0.06}_{-0.08}$	$2.76^{+0.10}_{-0.13}$	-1.11 ± 0.05
130606A	5.913		$3.31^{+0.12}_{-0.08}$	$-10.92^{+0.05}_{-0.06}$	$3.49^{+0.11}_{-0.15}$	-2.49 ± 0.33
130907A	1.238	*b*	$2.94^{+0.01}_{-0.01}$	$-7.72^{+0.01}_{-0.01}$	$2.53^{+0.01}_{-0.01}$	-1.66 ± 0.01
130925A	0.347		$2.39^{+0.02}_{-0.02}$	$-10.33^{+0.03}_{-0.03}$	$4.59^{+0.04}_{-0.05}$	-1.31 ± 0.03
131108A	2.4		$3.06^{+0.01}_{-0.01}$	$-10.61^{+0.08}_{-0.10}$	$3.44^{+0.11}_{-0.15}$	-1.89 ± 0.15
140304A	5.283		$3.07^{+0.08}_{-0.09}$	$-9.21^{+0.05}_{-0.06}$	$2.48^{+0.12}_{-0.16}$	-1.93 ± 0.22
140419A	3.956		$3.16^{+0.11}_{-0.15}$	$-9.27^{+0.03}_{-0.03}$	$2.39^{+0.04}_{-0.05}$	-1.43 ± 0.03
140423A	3.26		$2.73^{+0.03}_{-0.03}$	$-10.25^{+0.07}_{-0.09}$	$2.97^{+0.11}_{-0.15}$	-1.45 ± 0.09
140506A	0.889		$2.43^{+0.10}_{-0.13}$	$-9.59^{+0.07}_{-0.08}$	$2.79^{+0.09}_{-0.11}$	-1.13 ± 0.03
140512A	0.725		$3.01^{+0.06}_{-0.07}$	$-8.84^{+0.02}_{-0.02}$	$2.80^{+0.04}_{-0.04}$	-1.29 ± 0.02
140518A	4.707		$2.40^{+0.07}_{-0.08}$	$-10.61^{+0.05}_{-0.06}$	$2.89^{+0.17}_{-0.28}$	-2.19 ± 0.56
140629A	2.275	*f*	$2.45^{+0.08}_{-0.10}$	$-9.53^{+0.02}_{-0.02}$	$2.47^{+0.05}_{-0.06}$	-1.63 ± 0.06
140703A	3.14		$2.86^{+0.03}_{-0.04}$	$-9.83^{+0.07}_{-0.08}$	$2.64^{+0.15}_{-0.22}$	-1.73 ± 0.27
140907A	1.21	*b*	$2.40^{+0.03}_{-0.03}$	$-9.05^{+0.15}_{-0.22}$	$1.64^{+0.19}_{-0.34}$	-1.07 ± 0.04
141220A	1.3195		$2.62^{+0.02}_{-0.02}$	$-8.54^{+0.19}_{-0.34}$	$1.34^{+0.21}_{-0.41}$	-1.37 ± 0.07
141221A	1.452	*c*	$2.57^{+0.07}_{-0.09}$	$-9.58^{+0.12}_{-0.17}$	$2.24^{+0.15}_{-0.23}$	-1.18 ± 0.06
150120B	3.5		$2.77^{+0.33}_{-0.21}$	$-10.19^{+0.12}_{-0.16}$	$2.21^{+0.18}_{-0.31}$	-1.32 ± 0.13
150206A	2.087	*e*	$2.85^{+0.07}_{-0.07}$	$-10.89^{+0.06}_{-0.07}$	$4.34^{+0.09}_{-0.12}$	-1.87 ± 0.12
150314A	1.758	*d*	$2.93^{+0.01}_{-0.01}$	$-8.03^{+0.02}_{-0.02}$	$1.73^{+0.02}_{-0.02}$	-1.38 ± 0.01
150323A	0.593		$1.99^{+0.06}_{-0.07}$	$-10.98^{+0.07}_{-0.08}$	$3.80^{+0.16}_{-0.26}$	-1.48 ± 0.19
150403A	2.06	*e*	$3.06^{+0.07}_{-0.06}$	$-8.32^{+0.01}_{-0.01}$	$2.42^{+0.01}_{-0.01}$	-1.40 ± 0.01
150821A	0.755		$2.75^{+0.02}_{-0.02}$	$-10.00^{+0.23}_{-0.54}$	$3.28^{+0.30}_{-1.86}$	-1.27 ± 0.18
151021A	2.33	*f*	$2.75^{+0.06}_{-0.05}$	$-9.19^{+0.14}_{-0.20}$	$2.36^{+0.14}_{-0.21}$	-1.41 ± 0.05
151027A	0.81		$2.79^{+0.07}_{-0.09}$	$-9.17^{+0.01}_{-0.01}$	$3.65^{+0.03}_{-0.04}$	-2.32 ± 0.09
151111A	3.5		$2.68^{+0.03}_{-0.03}$	$-10.59^{+0.09}_{-0.12}$	$2.75^{+0.16}_{-0.27}$	-1.63 ± 0.21
160227A	2.38		$2.35^{+0.10}_{-0.12}$	$-11.42^{+0.04}_{-0.04}$	$4.91^{+0.10}_{-0.13}$	-2.53 ± 0.32
160509A	1.17	*b*	$2.90^{+0.01}_{-0.01}$	$-10.03^{+0.03}_{-0.03}$	$4.28^{+0.06}_{-0.07}$	-1.74 ± 0.08
160625B	1.406	*c*	$3.20^{+0.01}_{-0.01}$	$-9.09^{+0.11}_{-0.16}$	$3.25^{+0.11}_{-0.14}$	-1.46 ± 0.03
160804A	0.736		$2.11^{+0.02}_{-0.02}$	$-11.07^{+0.05}_{-0.06}$	$3.79^{+0.12}_{-0.17}$	-1.07 ± 0.08
161017A	2.0127	*e*	$2.95^{+0.06}_{-0.07}$	$-10.37^{+0.04}_{-0.04}$	$3.69^{+0.06}_{-0.07}$	-2.12 ± 0.11
161117A	1.549		$2.24^{+0.02}_{-0.02}$	$-10.26^{+0.05}_{-0.06}$	$3.33^{+0.08}_{-0.10}$	-1.26 ± 0.06
161219B	0.1475		$2.02^{+0.09}_{-0.11}$	$-9.63^{+0.02}_{-0.02}$	$3.52^{+0.03}_{-0.04}$	-1.01 ± 0.01
170113A	1.968		$2.34^{+0.16}_{-0.27}$	$-9.89^{+0.04}_{-0.04}$	$2.79^{+0.06}_{-0.07}$	-1.36 ± 0.05
170202A	3.645		$3.06^{+0.22}_{-0.19}$	$-10.38^{+0.07}_{-0.08}$	$2.77^{+0.12}_{-0.17}$	-1.08 ± 0.09
170405A	3.51		$3.20^{+0.01}_{-0.01}$	$-9.80^{+0.05}_{-0.06}$	$2.54^{+0.11}_{-0.15}$	-1.53 ± 0.14
170604A	1.329		$2.71^{+0.12}_{-0.11}$	$-10.08^{+0.08}_{-0.09}$	$3.29^{+0.12}_{-0.16}$	-1.54 ± 0.10
170607A	0.557	*a*	$2.38^{+0.04}_{-0.04}$	$-10.50^{+0.03}_{-0.03}$	$4.06^{+0.06}_{-0.06}$	-1.20 ± 0.04
170705A	2.01	*e*	$2.67^{+0.08}_{-0.07}$	$-10.17^{+0.02}_{-0.03}$	$3.43^{+0.04}_{-0.04}$	-1.27 ± 0.02
171010A	0.3285		$2.31^{+0.01}_{-0.01}$	$-10.30^{+0.07}_{-0.08}$	$4.59^{+0.10}_{-0.13}$	-1.93 ± 0.13
171205A	0.0368		$2.10^{+0.28}_{-0.13}$	$-11.86^{+0.05}_{-0.06}$	$5.30^{+0.13}_{-0.19}$	-1.00 ± 0.09
180205A	1.409	*c*	$2.31^{+0.07}_{-0.08}$	$-9.63^{+0.19}_{-0.33}$	$2.03^{+0.22}_{-0.49}$	-1.08 ± 0.06
180325A	2.248	*f*	$2.30^{+0.07}_{-0.06}$	$-9.17^{+0.03}_{-0.03}$	$3.11^{+0.05}_{-0.05}$	-3.02 ± 0.17
180329B	1.998	*e*	$2.16^{+0.07}_{-0.09}$	$-10.61^{+0.03}_{-0.03}$	$3.46^{+0.07}_{-0.09}$	-1.81 ± 0.15
180620B	1.1175	*b*	$2.50^{+0.03}_{-0.03}$	$-10.35^{+0.04}_{-0.04}$	$3.97^{+0.08}_{-0.10}$	-1.48 ± 0.09
180720B	0.654		$3.02^{+0.01}_{-0.01}$	$-8.21^{+0.01}_{-0.01}$	$3.06^{+0.02}_{-0.02}$	-1.47 ± 0.01
180728A	0.117		$1.95^{+0.01}_{-0.01}$	$-8.68^{+0.01}_{-0.01}$	$3.33^{+0.02}_{-0.02}$	-1.30 ± 0.01
181010A	1.39		$2.83^{+0.11}_{-0.15}$	$-9.63^{+0.04}_{-0.05}$	$2.48^{+0.07}_{-0.08}$	-1.25 ± 0.04
181020A	2.938		$3.16^{+0.02}_{-0.02}$	$-8.51^{+0.03}_{-0.03}$	$1.91^{+0.03}_{-0.04}$	-1.69 ± 0.03
181110A	1.505	*c*	$2.08^{+0.11}_{-0.36}$	$-10.05^{+0.05}_{-0.06}$	$3.13^{+0.08}_{-0.10}$	-1.67 ± 0.12

Note. GRBs belonging to the sub-samples at $\langle z \rangle \approx 0.54$, 1.18, 1.46, 1.70, 2.05, 2.27, and 2.69 are labeled by *a*, *b*, *c*, *d*, *e*, *f*, and *g*, respectively. Errors are at 1σ confidence level.

(This table is available in machine-readable form.)

ORCID iDs

M. Muccino https://orcid.org/0000-0002-2234-9225
L. Izzo https://orcid.org/0000-0001-9695-8472
O. Luongo https://orcid.org/0000-0001-7909-3577
K. Boshkayev https://orcid.org/0000-0002-1385-270X
L. Amati https://orcid.org/0000-0001-5355-7388
M. Della Valle https://orcid.org/0000-0003-3142-5020
G. B. Pisani https://orcid.org/0000-0003-3452-2491

References

Amanullah, R., Lidman, C., Rubin, D., et al. 2010, ApJ, 716, 712
Amati, L., D'Agostino, R., Luongo, O., Muccino, M., & Tantalo, M. 2019, MNRAS, 486, L46
Amati, L., & Della Valle, M. 2013, IJMPD, 22, 1330028
Amati, L., Guidorzi, C., Frontera, F., et al. 2008, MNRAS, 391, 577
Amati, L., O'Brien, P., Götz, D., et al. 2018, AdSpR, 62, 191
Aviles, A., Bravetti, A., Capozziello, S., & Luongo, O. 2014, PhRvD, 90, 043531
Aviles, A., Gruber, C., Luongo, O., & Quevedo, H. 2012, PhRvD, 86, 123516
Bernardini, M. G., Margutti, R., Zaninoni, E., & Chincarini, G. 2012, MNRAS, 425, 1199
Bronstein, M. P. 1933, UsAsT, 3, 3
Bryant, C., Osborne, J. A., & Shahmoradi, A. 2020, arXiv:2010.02935
Caldwell, R. R. 2002, PhLB, 545, 23
Caldwell, R. R., Kamionkowski, M., & Weinberg, N. N. 2003, PhRvL, 91, 071301
Capozziello, S., D'Agostino, R., & Luongo, O. 2019, IJMPD, 28, 1930016
Capozziello, S., D'Agostino, R., & Luongo, O. 2020, MNRAS, 494, 2576
Capozziello, S., & Izzo, L. 2008, A&A, 490, 31
Chevallier, M., & Polarski, D. 2001, IJMPD, 10, 213
Cordier, B., Götz, D., Motch, C. & SVOM Collaboration 2018, MmSAI, 89, 266
Coward, D. M., Howell, E. J., Branchesi, M., et al. 2013, MNRAS, 432, 2141
Cucchiara, A., Levan, A. J., Fox, D. B., et al. 2011, ApJ, 736, 7
D'Agostini, G. 2005, arXiv:physics/0511182
Dainotti, M. G., Cardone, V. F., & Capozziello, S. 2008, MNRAS, 391, L79
Dainotti, M. G., Postnikov, S., Hernandez, X., & Ostrowski, M. 2016, ApJL, 825, L20
Daly, R. A., & Djorgovski, S. G. 2004, ApJ, 612, 652
Ding, X., Biesiada, M., Cao, S., Li, Z., & Zhu, Z.-H. 2015, ApJL, 803, L22
Goobar, A., & Perlmutter, S. 1995, ApJ, 450, 14
Gruber, C., & Luongo, O. 2014, PhRvD, 89, 103506
Huterer, D., & Cooray, A. 2005, PhRvD, 71, 023506
Izzo, L., Capozziello, S., Covone, G., & Capaccioli, M. 2009, A&A, 508, 63
Izzo, L., Luongo, O., & Capozziello, S. 2012, MSAIS, 19, 37
Izzo, L., Muccino, M., Zaninoni, E., Amati, L., & Della Valle, M. 2015, A&A, 582, A115
King, A. L., Davis, T. M., Denney, K. D., Vestergaard, M., & Watson, D. 2014, MNRAS, 441, 3454
Linder, E. V. 2003, PhRvL, 90, 091301
Luongo, O., & Muccino, M. 2020a, A&A, 641, A174
Luongo, O., & Muccino, M. 2020b, arXiv:2011.13590
Margutti, R., Zaninoni, E., Bernardini, M. G., et al. 2013, MNRAS, 428, 729
Muccino, M., & Boshkayev, K. 2017, MNRAS, 468, 570
Perlmutter, S., Aldering, G., della Valle, M., et al. 1998, Natur, 391, 51
Perlmutter, S., Aldering, G., Goldhaber, G., et al. 1999, ApJ, 517, 565
Phillips, M. M. 1993, ApJL, 413, L105
Planck Collaboration, Aghanim, N., Akrami, Y., et al. 2020, A&A, 641, A6
Riess, A. G., Casertano, S., Yuan, W., Macri, L. M., & Scolnic, D. 2019, ApJ, 876, 85
Riess, A. G., Filippenko, A. V., Challis, P., et al. 1998, AJ, 116, 1009
Riess, A. G., Strolger, L.-G., Casertano, S., et al. 2007, ApJ, 659, 98
Risaliti, G., & Lusso, E. 2019, NatAs, 3, 272
Rodney, S. A., Riess, A. G., Scolnic, D. M., et al. 2015, AJ, 150, 156
Ruffini, R., Muccino, M., Bianco, C. L., et al. 2014, A&A, 565, L10
Sahni, V., Shafieloo, A., & Starobinsky, A. A. 2014, ApJL, 793, L40
Salvaterra, R., Campana, S., Vergani, S. D., et al. 2012, ApJ, 749, 68
Schaefer, B. E. 2007, ApJ, 660, 16
Schmidt, B. P., Suntzeff, N. B., Phillips, M. M., et al. 1998, ApJ, 507, 46
Stratta, G., Dainotti, M. G., Dall'Osso, S., Hernandez, X., & De Cesare, G. 2018, ApJ, 869, 155
Suzuki, N., Rubin, D., Lidman, C., et al. 2012, ApJ, 746, 85
Tang, C.-H., Huang, Y.-F., Geng, J.-J., & Zhang, Z.-B. 2019, ApJS, 245, 1
Tsujikawa, S. 2013, CQGra, 30, 214003
Velten, H., & Gomes, S. 2020, PhRvD, 101, 043502
Wei, J.-J., & Melia, F. 2020, ApJ, 888, 99
Wei, J.-J., Wu, X.-F., Melia, F., Wei, D.-M., & Feng, L.-L. 2014, MNRAS, 439, 3329
Xu, F., Tang, C.-H., Geng, J.-J., et al. 2020, arXiv:2012.05627
Yang, T., Banerjee, A., & Colgáin, E. Ó. 2020, PhRvD, 102, 123532
Zhang, S. N., Feroci, M., Santangelo, A., et al. 2016, Proc. SPIE, 9905, 99051Q